Interaction between an Advancing Shock Wave and Opposing Jet Flow

THOMAS M. WEEKS* AND DARSHAN S. DOSANJH†
Syracuse University, Syracuse, N. Y.

The interaction between a plane shock wave advancing in a shock tube and an opposing axisymmetric jet flow was recorded experimentally and analyzed. Shadowgraph, schlieren, and interferometric observations revealed that the shape of the shock distortion (bulge) caused by the jet flow closely resembled that of the local jet mean velocity distribution. Oblique shock relations, applied across shock bulge segments, yielded local flow jump parameters. The density distribution thus obtained compared favorably with interferometric results. Beginning at the bulge apex as a maximum the flow field exhibited several adjacent density maxima and minima in the axial direction. Within 1½ and 10 nozzle diameters in the radial and axial direction, respectively, these oscillations attenuated, and the density approached the uniform value observed behind the undisturbed normal main shock front. Applying mass and momentum conservation relations and assuming isentropic processes in the axial direction, corresponding flow field quantities were obtained. An intense, intermittent compression wave system with wavelength nearly equal to the jet diameter appeared behind the moving shock front. The intensity of the propagating discrete wavelets was found to be of the order of 170 db and was observed to diminish in accordance with moving point-source emission theory.

Nomenclature

a = speed of sound
b = jet mixing zone width
c = jet core radius
d = jet nozzle diameter
I = intensity of compression waves
k = optical constant (0.000292)
l = shock bulge amplitude
l_R = decibel scale intensity of compression waves
L = test section width
M = Mach number
N = fringe jump number
p = pressure
P_i = emission point of wavelet W_i
r = radial distance from jet axis
r_i = distance from point P_i to wavelet W_i
r_{lm} = radius corresponding to one-half maximum shock bulge amplitude
r_m = radius corresponding to one-half maximum jet mean velocity
r_0 = limiting radius of interferometric analysis
S = shock strength = p_{2u}/p_{1u}
T = absolute temperature
u = particle velocity in x direction
U_e = jet exit velocity
U_s = shock speed
v = particle velocity in r direction
W_i = ith wavelet
x = axial distance from nozzle exit
x' = axial distance from shock bulge apex towards nozzle exit
z = direction of light path through test section
β = shock bulge slope angle
θ = angle between direction of emission and direction of motion of emitting point P_i
λ = wavelength of light
λ_R = radiation wavelength
ρ = density
ω = frequency of discrete radiation = a_{2u}/λ_R

Subscripts

0 = stagnation conditions
1 = ahead of shock wave
2 = behind shock wave
$1j,2j$ = jet flow conditions ahead of and behind shock wave, respectively
$1u,2u$ = uniform conditions ahead of and behind shock wave, respectively

Received by IAS December 3, 1962; revision received April 26, 1963. The work described in this paper was supported by the U. S. Army Research Office, Durham Contract DA-30-115-ORD-893 and Grant DA-ARO(D)-31-124-G210. Grateful acknowledgment is extended to William Sheeran for his assistance in the operation of the experimental facility. Darshan S. Dosanjh is pleased to acknowledge the time he spent writing the paper while he was a visiting professor at the College of Aeronautics, Cranfield, England.

* Graduate Student in Mechanical Engineering, L. C. Smith College of Engineering.

† Professor of Mechanical Engineering, L. C. Smith College of Engineering. Member AIAA.

Introduction

THE concurrence of shock waves and fluctuations or disturbances in high-speed flow systems is experienced commonly. The convection of these disturbances through the shock waves plays an important role in a variety of gasdynamics and aerodynamics problems and has formed the subject of a number of recent investigations. Lighthill[1] analyzed the scattering of energy when sound or weak shock waves pass through turbulent flow. Ribner[2,3] studied the convection of a pattern of vorticity and also the passage of a single vortex through a shock front. Werner[4] extended the analysis to the convection of a bounded cellular vortex field as well as a single column of vortex cells through a shock wave and predicted the transient behavior (distortion) of the shock wave and pressure disturbances generated downstream of the shock front.

Powell[5,6] established that noise characteristics (frequency, intensity, and directionality) of jet flows markedly change above choking, i.e., when shock waves appear in turbulent jet flows. The continuous frequency noise spectrum then is dominated by a powerful whistle or screech whose wavelength (or frequency) is related to the regular shock pattern through which the upstream flow disturbances are convected.

Another class of problems, which has gained some practical importance, involves the interaction of a shock wave with an injected jet flow. Such an interaction takes place when a forward-facing jet flow is injected from the blunt nose of a hypersonic re-entry vehicle. This has been investigated as a possible means of alleviating the heat transfer problem[7] but apparently results in an increased rate of convective heat

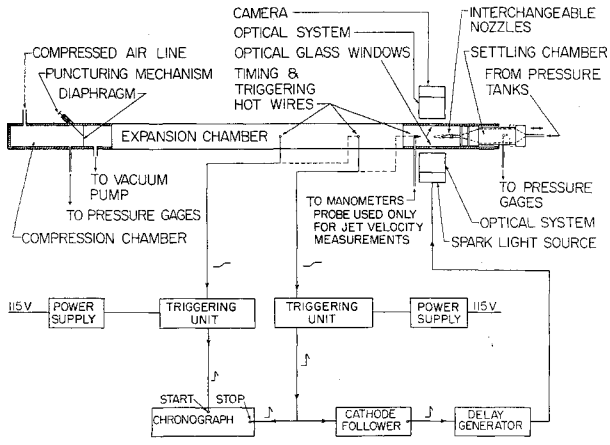

Fig. 1 Block diagram of experimental facility

transfer to the vehicle.[8] As another example, if a re-entry vehicle was to be decelerated within the earth's atmosphere by means of a high-thrust retrorocket, the rocket exhaust would interact with the standing bow shock front.[9] Such jet flow-shock interactions are known to result in the displacement and distortion of the bow shock.[10] In these flow configurations the jet is directed from high to low pressure side of the shock front. In close formation supersonic flight, the jet exhaust of the leading aircraft may interact with the body shock waves of the one following. Here the jet flow is directed from the low to the high pressure side of the shock front. It is apparent that if relative motion between these aircraft takes place a problem akin to propagating shock-jet flow interaction arises.

Similar interactions between a traveling shock front and turbulent jet flows were investigated experimentally in a shock tube by Dosanjh.[11] In his experiments an axisymmetric jet was directed, in one case, from the high to the low pressure side of a receding shock front and, in another, from the low to the high pressure side of an advancing shock front. In both cases distortion of the shock front occurred. In addition, in the latter case, an intense intermittent high-frequency radiation appeared in the flow field behind the shock front. Dosanjh pointed out that the wavelength of the wavelets was nearly equal to the nozzle diameter (or local jet flow diameter).

Dosanjh's experiments were conducted, however, with a single nozzle diameter and shock strength. The optical data were entirely shadowgraphic, yielding only qualitative details of the flow field behind the shock front. Therefore, further experimental investigations of the interaction between a traveling shock wave and opposing jet flow were undertaken to extend systematically the earlier investigations including additional nozzle diameters, shock strengths, jet exit velocities (subsonic and choked), and x/d locations of the shock front from the nozzle exit. The shock-jet flow interactions were recorded using shadowgraph, schlieren, and interferometer techniques. The nature of the local shock distortion, interaction field density distribution, and the discrete wavelet radiation (wavelength, strength, and attenuation) was investigated.

Applying oblique shock relations, the local flow jump conditions across shock segments were obtained. The results were compared with the interferometrically determined density distribution.

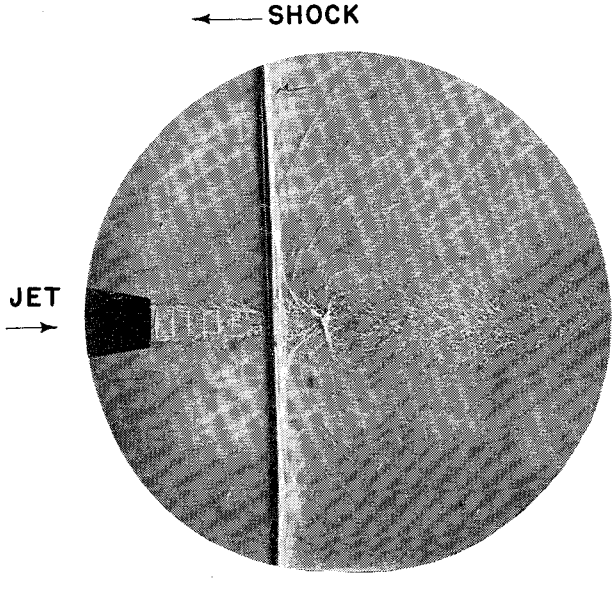

Fig. 2 Traveling shock-opposing axisymmetric jet interaction; $S = 1.46$, $x/d = 3.20$; choked jet: $p_{01j}/p_{1u} = 2.00$, $d = \frac{1}{4}$ in., $T_{01j} = 73°\text{F}$

Experimental Facility

A 6-in.^{2} cross section, 24-ft-long steel shock tube, with a 4-in.-diam optical glass window located 15 ft from the dia-

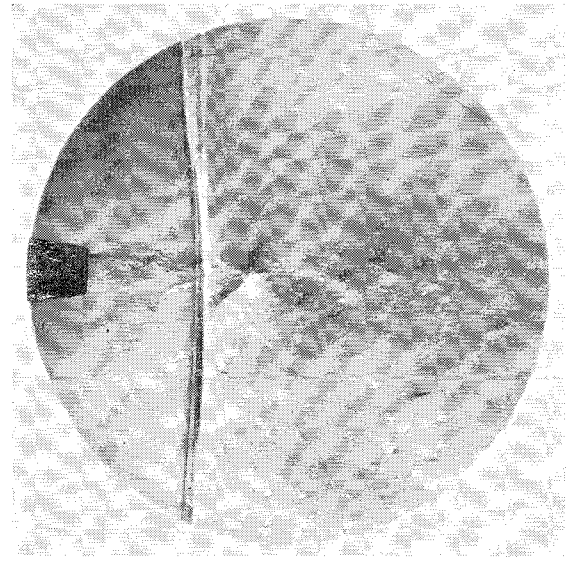

a) Schlieren horizontal knife edge

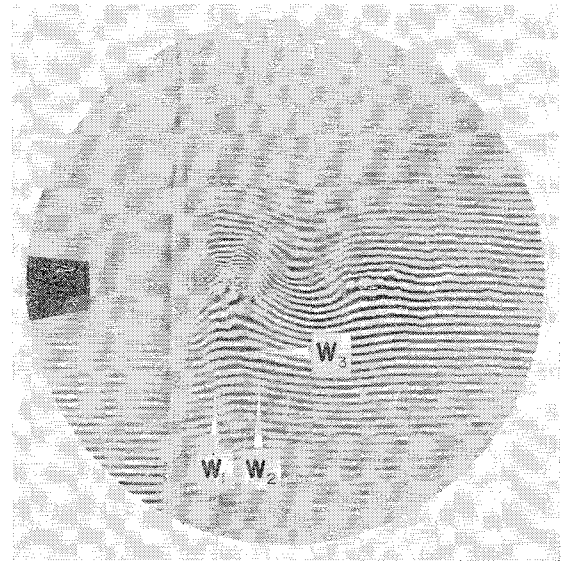

b) Monochromatic interferogram

Fig. 3 Traveling shock-opposing axisymmetric jet interaction; $S = 1.46$, $x/d = 3.00$; subsonic jet: $p_{01j}/p_{1u} = 1.87$, $U_e \approx 1100$ fps, $d = \frac{1}{4}$ in., $T_{01j} = 74°\text{F}$

phragm was used in these investigations (Fig. 1). Shock speeds (and, therefore, strengths) were obtained from the measured time of transit of the shock front between two hot wire transducers placed 3 ft apart.[12]

The compressed air supply (maximum pressure, 350 psig; total storage volume, 450 ft^3) was dried, filtered, and regulated to maintain various constant jet settling chamber pressures for a wide range of mass flow rates. Axisymmetric converging nozzles with $\frac{1}{4}$-in., $\frac{1}{2}$-in., and 1-in. diameters were mounted individually in the center of the shock tube in a direction opposite to that of the advancing shock front. Preliminary investigations used an arrangement in which the far end of the shock tube was open and the jet efflux accumulating in the expansion chamber flowed out the open end. Here, the jet flow was surrounded by an opposing back flow which resulted in additional distortion of the shock front. This problem was alleviated by exhausting the expansion chamber with a rotary piston vacuum pump (Fig. 1), the exhaust rate being adjusted to establish the desired pressure (usually atmospheric).

Experimental Procedures and Conditions

Traveling shock-opposing axisymmetric jet interactions were recorded interferometrically. The shock strength S was varied from 1.27 to 2.0, and the jet was operated at exit velocities ranging from subsonic ($U_e = 350$ fps) to choked with p_{01j}/p_{1u} as high as 2.36. The relative position of the shock front and nozzle exit was varied from $x/d = 0.74$ to 12. Monochromatic and white light interferograms were recorded simultaneously using a filtered (448 mμ) and unfiltered single magnesium spark. Some of the experimental runs were repeated adapting the interferometer as shadowgraph and schlieren systems. Typical examples appear in Figs. 2 and 3. Additional details of the construction and operation of the shock tube and associated systems are available in Ref. 13.

Glass slides of the interferograms were scanned using an optical comparator, and the fringe locations at constant x/d stations were obtained. An IBM 650 Fortran program was written to solve Abel's integral

$$N = \frac{k}{\lambda}\int_0^L \frac{\rho - \rho_{1u}}{\rho_{1u}}\,dz$$

The assumption of axial symmetry led to the employment of the constant density annular zone method. The zones were chosen such that consecutive zone radii corresponded to consecutive fringe positions on the interferogram. Thus the geometrical zone coefficients as well as the density field were obtained with a single computer program using the raw fringe location data directly.‡ It should be noted that this method can be extended only to a radius $r = r_0$ of the innermost observable fringe. For additional details, see Refs. 13 and 14.

The optical records of shock-opposing jet interaction revealed three distinct flow phenomena: 1) The opposing jet flow distorts the advancing shock front. 2) The jet flow and the drift flow behind the shock wave are modified by the interaction. 3) A discrete wave system is generated behind the shock front.

‡ The integration procedure required in analyzing shock-axisymmetric jet interactions is tedious and subject to some degree of error. It, therefore, appeared desirable to use a two-dimensional ($\frac{1}{8}$-in.) wall to wall jet mounted in the arrangement of Fig. 1. It was found, however, that because of Coanda-type entrainment asymmetry the jet deflected toward either the top or bottom wall. A mounting arrangement with the far end of the shock tube open resulted in oscillatory deflection of the jet flow. Therefore, the resultant jet flow field in both cases was unsatisfactory to shock-jet interaction studies. For additional details of the difficulties encountered, see Refs. 13 and 14.

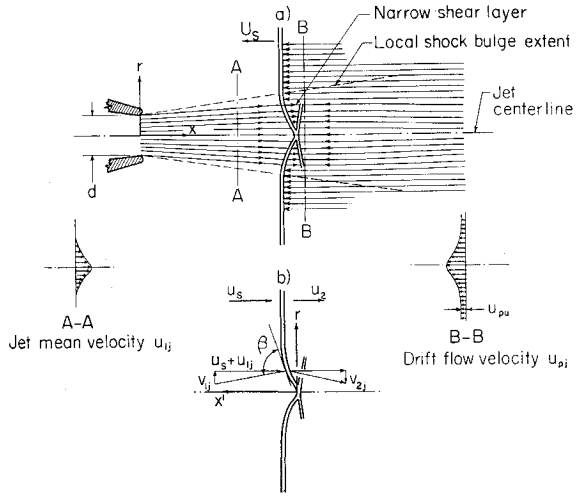

Fig. 4 Sketch of propagating shock-opposing jet interaction; coordinates fixed on a) jet nozzle, b) advancing shock

Shock Distortion

The local shock distortion caused by the opposing jet is in the form of a bulge depression bearing a striking resemblance to the jet mean velocity profile just ahead of it. For example, when the shock front is located in the free-turbulence (similarity) region of the jet flow, the bulge shape is nearly Gaussian (Fig. 3). As the shock wave progresses into the potential core-mixing region, the shock bulge develops a normal portion the size of the local jet potential core, and the surrounding portion of the shock bulge profile still resembles the local jet mean velocity profile. A careful examination of optical data revealed that the turbulent nature of the jet flow caused only secondary local distortion of the shock bulge.

In order to predict the shape of the shock bulge theoretically, it is necessary to know the flow properties behind as well as ahead of the shock front. The flow properties behind the shock bulge, however, depend upon its shape. This nonlinear interdependence of the "shocked" jet flow and the shock bulge shape complicates any theoretical analysis.[4] A first-order approximation was derived assuming that the shock bulge adjusts itself such that uniform pressure conditions are achieved immediately behind the shock front (i.e., $p_{2j} = p_{2u}$). Experimental observations revealed, however, that immediately behind the shock bulge the pressure is higher than the uniform value p_{2u} but attains this value approximately 1 nozzle diameter downstream. The analysis was based entirely on the mean flow properties (see Fig. 4 for notation). Viscous effects were neglected. The equations of motion were written for flow conditions both outside and inside the jet flow region in a coordinate system fixed on the moving shock front (Fig. 4b). These equations reduce to a single differential equation describing the shock bulge slope:

$$\tan\beta = \frac{dr}{dx'} = \frac{\rho_{1j}v_{1j}^2 - \rho_{1u}U_s^2}{\rho_{1j}(U_s + u_{1j})v_{1j} \pm [\rho_{1j}(U_s + u_{1j})v_{1j}]^2 - [\rho_{1j}(U_s + u_{1j})^2 - \rho_{1u}U_s^2][\rho_{1j}v_{1j}^2 - \rho_{1u}U_s^2]^{1/2}} \quad (1)$$

Details of the derivation of Eq. (1) appear in Ref. 13. If $v_{1j} \ll (u_{1j};\ U_s)$, then

$$dr/dx' \approx \{[\rho_{1j}(U_s + u_{1j})^2/\rho_{1u}U_s^2] - 1\}^{-1/2} \quad (2)$$

For incompressible jet flow $\rho_{1j} = \rho_{1u}$, Eq. (2) becomes

$$dr/dx' \approx \{[(U_s + u_{1j})/U_s]^2 - 1\}^{-1/2}$$

or

$$\sin\beta \approx U_s/(U_s + u_{1j}) = M_{1u}/M_{1j} \quad (3)$$

Thus the simplifying assumptions $v_{1j} \ll (u_{1j};\ U_s)$ and $\rho_{1j} = \rho_{1u}$ reduce Eq. (2) to the well-known correspondence between normal and oblique shocks having the same strength.

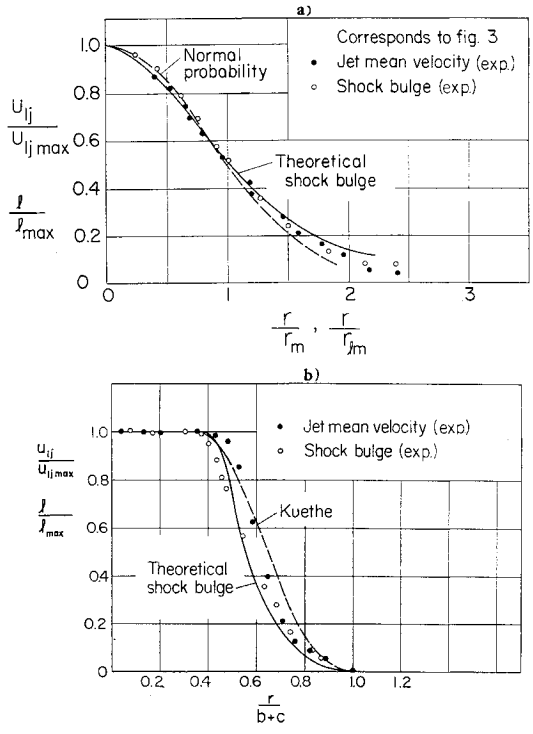

Fig. 5 Nondimensional jet mean velocity and shock bulge profiles

From Eq. (2) it is apparent that in the absence of jet flow ($u_{1j} = 0$) the slope dr/dx' of the shock front becomes infinite (normal shock), and for $u_{1j} > 0$ the shock bulge slope takes on finite values. However, in the potential core region of the jet flow where $u_{1j} = U_e$, the central portion of the shock bulge is observed experimentally to be normal, i.e., its slope is infinite. Therefore, Eq. (2) does not describe the shock bulge slope in the potential core region. Additionally, in this analysis the shock bulge can be no wider than the jet flow. However, the shock bulge is observed experimentally to extend beyond the jet boundaries (Figs. 2 and 3). This discrepancy may be attributed to the fact that, as the shock front advances toward the jet exit, it passes through a progressively narrowing jet cross section. If the adjustment of the shock bulge to the local jet extent is slower than the rate of decrease of jet width, the shock bulge will appear wider than the local jet flow. Also, on the jet boundary, at a given instant, the junction of the oblique shock contained in the jet flow region and the main normal shock front must smoothen due to the viscous effects. This also will cause the shock bulge to extend beyond the local jet flow boundaries.

If the local jet velocity distribution for two-dimensional or axisymmetric jets is prescribed just ahead of the shock bulge, then Eq. (2) can be integrated. For shock locations in the free-turbulence portion of the axisymmetrical jet, the Gaussian mean velocity distribution[15]

$$u_{1j}/U_e = C_1 \exp C_2(-r^2/x^2) \tag{4}$$

was used in Eq. (2). Nondimensional plots of this jet mean velocity distribution and the numerical integration of Eq. (2) are presented in Fig. 5a. In the case of the shock located within the potential core-mixing region the velocity distribution

$$u_{1j}/U_e = \{1 - [(r - c)/b]^{2/3}\}^2 \tag{5}$$

was chosen after Kuethe,[16] where constants c and b are determined experimentally (see Fig. 5b). It can be seen that in both cases agreement is fair, justifying the first-order approximation for the shape of the shock bulge in the jet mixing region (surrounding the potential core) as well as in the similarity region.

An additional oblique shock surface was observed to form at the bulge apex extending toward the jet boundary to about the size of the nozzle diameter (Fig. 2). In the case of shock locations in the free turbulence portion of the jet, the extended shock originated at the bulge apex, and the resulting configuration resembled the diamond shock cell pattern in a choked jet. For shock locations within the potential core-mixing region the extended shock surface originated at the normal shock disk circumference, and flow calculations confirmed the presence of the observed slipstream originating at the triple point.

Flow Field behind Shock Bulge

The analysis of numerous interferograms of shock-jet interaction was carried out in order to evaluate the nature of the overall density field behind the shock front. Values of the density ratio ρ_2/ρ_1 were obtained at several locations downstream of the shock front as a function of radial distance r. For example, the radial and axial variations of the density ratio ρ_2/ρ_1 (corresponding to Fig. 3) are presented in Figs. 6a and 6b, respectively. The characteristic shape of these curves is typical of other interactions as well. For clarity only a few curves are presented in each plot. It is apparent that, beyond 1.5 nozzle diameters from the jet axis and 10 nozzle diameters downstream from the shock location, the density ratio assumed the uniform value ρ_{2u}/ρ_{1u} which is slightly lower (no more than 1%) than that predicted by shock speed measurements. This negligible difference may be attributed to a slight decrease in shock strength caused by the nonuniform flow present between the last timing station and actual interaction location (a distance of about 3.5 ft). Closer to the jet axis (up to $r = r_0$) the density ratio ρ_2/ρ_1 is seen either to rise above or fall below the shock alone value ρ_{2u}/ρ_{1u}. In the axial plot, Fig. 6b, a high-density region

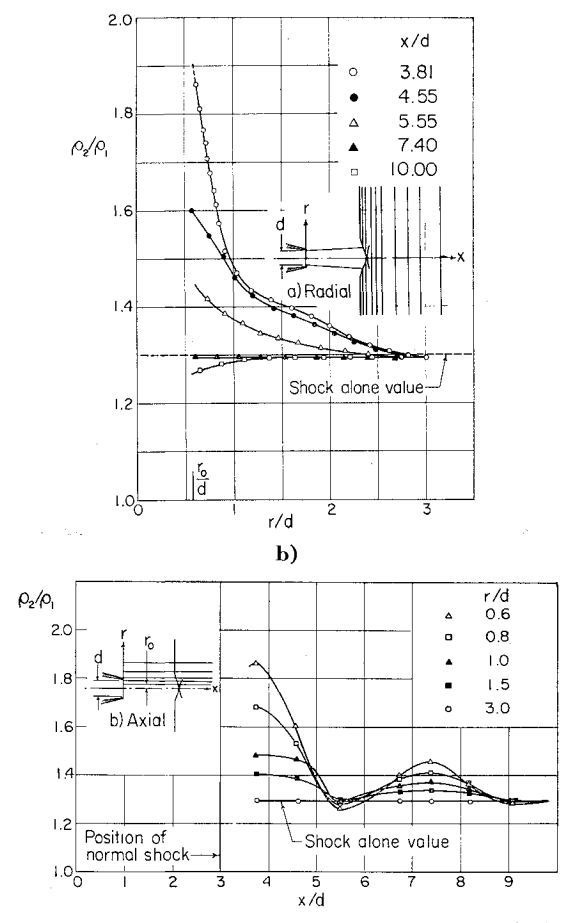

Fig. 6 Typical density distribution behind shock (interferogram Fig. 3); a) radial, b) axial

forms at the shock bulge apex, followed axially by a region of decreasing density attaining a minimum about 2 nozzle diameters from the location of the maximum. This is followed by an increase in density, another relative maximum, and so on. The distance between adjacent maxima or minima is of the order of 4 nozzle diameters. The local upstream velocity u_{1j} and the local shock bulge angle β were measured, and the corresponding upstream temperature $T_{1j} \propto (u_{1j})^{1/2}$ was obtained. Across local segments of the shock bulge oblique shock relations were applied, and the density, pressure, and temperature ratios (ρ_2/ρ_1, p_2/p_1, T_2/T_1) were calculated. The density ratio thus obtained was compared to the interferometric values (Fig. 7). In Fig. 7a (corresponding to Fig. 3) the shock location is in the free-turbulence portion of the jet. In Fig. 7b the shock front is located in the potential core-mixing region of the jet. The dashed line in the inset indicates the position at which ρ_2/ρ_1 was evaluated. The comparison reveals that the density ratio found from oblique shock relations falls below that obtained from the interferometric analysis by about 10%. Further examination of Fig. 7b reveals that, for the region between the jet flow boundary (b) at $r/d \approx 0.62$ and the shock bulge boundary (a) at $r/d = 1.1$, the density and pressure ratios determined from oblique shock relations fall below the uniform values ρ_{2u}/ρ_{1u} and p_{2u}/p_{1u}, respectively. The reason is that outside the jet flow boundary (i.e., no opposing flow) the oblique shock Mach number $U_s \sin\beta/a_{1u}$ is less than the corresponding normal shock Mach number U_s/a_{1u}. This density behavior is not evident from the interferometric observations, apparently due to the smoothening effect of the integration procedure. Since the accuracy of the results obtained both interferometrically and from oblique shock theory was estimated to be within about 5%, the agreement between the two methods is fairly good. On the basis of this agreement, the associated flow field characteristics were calculated. For the pressure distribution just behind the shock bulge, see Fig. 7. The appearance of a high-pressure region at the bulge apex is evident for shock locations in and downstream of the potential core. Farther downstream from the shock front, ap-

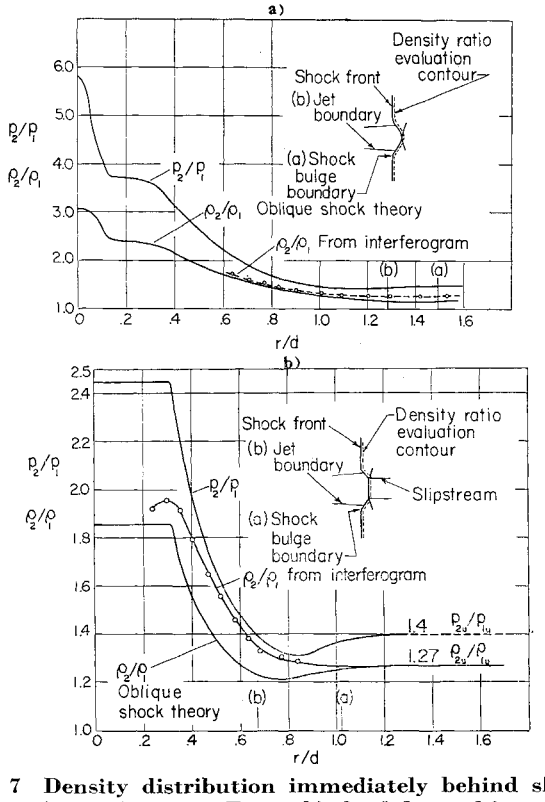

Fig. 7 Density distribution immediately behind shock front; a) interferogram Fig. 3, b) shock located in potential core

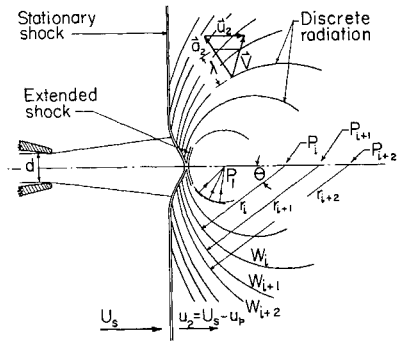

Fig. 8 Intermittent compression wave pattern behind shock front; upper portion, determination of average wavelength; lower portion, location of emission points

proximate flow characteristics were calculated using mass and momentum conservation relations and assuming isentropic processes in the axial direction. The streamlines and velocity profiles corresponding to Fig. 3 are shown in Fig. 4. In order to improve the accuracy, the initial streamline spacing was chosen somewhat narrower near the jet axis where larger mass flow gradients were present. It was found that the oblique shock bulge deflects the jet flow inward toward the axis. Since the drift flow following the oblique portion of the main shock front just outside the jet flow boundary is directed opposite to this deflected flow, a narrow shear layer develops. The extended conical shock surface returns the flow parallel to the jet axis and reverses the direction of flow behind it. The streamlines expand slightly, reaching a maximum spacing at the first density minimum, and then contract gradually to a uniform spacing farther downstream.

In the case of shock locations within the potential core a somewhat different flow field is established. The flow velocity u_{pj} behind the normal portion of the shock bulge is constant and is a function of the local shock Mach number $(U_s + U_e)/a_{1j}$. At the circumference of this normal shock disk, u_{pj} and density ratio ρ_{2j}/ρ_{1j} undergo a discontinuous increase at constant pressure and then decrease radially along the extended shock to the uniform values u_p and ρ_{2u}/ρ_{1u} behind the main normal shock. The flow remains parallel to the jet axis, directed towards the shock front. These calculations confirm the presence of the optically observed slipstream that forms at the triple point and extends a short distance downstream.

It was found that the pressure distribution at the first-density minimum section was constant and equal to the uniform value p_{2u} to within 4%. This suggests that the initial expansion from the shock bulge apex yields uniform pressure conditions, and, therefore, the subsequent density oscillations are accompanied by temperature oscillations at constant pressure. The assumption of a constant pressure process downstream of the first-density minimum, however, had no noticeable effect on the streamline spacing previously calculated on the basis of isentropic expansion.

Intermittent Wave Field

Another interesting characteristic of shock-jet interaction is the appearance of a clearly discernible, regularly spaced (discrete) system of propagating compression wavelets in the flow field behind the traveling shock front for both subsonic and supersonic opposing jet flows (Figs. 2, 3, 8). The compressive nature of the wavelets was established from interferograms (e.g., Fig. 3) where the fringe jump across the wavelets and the main shock front is in the same direction. This also was confirmed by the examination of schlieren photographs. In addition to the main wave system, a weaker pattern of numerous wavelets (apparently of higher frequency) also was

Table 1 Typical frequency and predominant wavelength of radiated wavelets

Jet diameter d, in.	Wavelength λ_R, in.	Frequency $\omega = \frac{a_{2u}}{\lambda_R}$, kc
0.25	0.24 ± 0.03	55.61
0.50	0.51 ± 0.03	29.02 } at $S = 1.46$
1.00	1.10 ± 0.03	14.50

observed. Only the discrete system was investigated for its predominant wavelength, frequency, and intensity.

It is worthwhile to point out that small fluctuations of the interference fringes in the jet flow region behind the advancing shock front are more pronounced than those ahead of the shock (Fig. 3). This suggests the possibility of an increase in the jet flow turbulence level as a result of shock-jet interaction. No quantitative measurements of this effect were undertaken.

a. Wavelength and frequency of radiated wavelets

The earlier suggestion by Dosanjh[11] that the predominant wavelength λ_R of the radiated wavelets may have a dependence upon the jet diameter was examined further in this investigation. Considering the shock front to be stationary and assuming the local propagation velocity of each wavelet to be the vector sum of the local speed of sound normal to the wave and the flow velocity bebind the shock u_2, a velocity-vector diagram was constructed at many points on each wavelet as shown in Fig. 8. For each shadowgraph an average value of the predominant wavelength λ_R was found to be nearly equal to the jet diameter, d, and almost independent of shock strength, jet exit velocity, and distance downstream from the nozzle exit.[13] An overall average value of λ_R was found for each jet diameter. The results are summarized in Table 1.

The discrete wave pattern was examined further to determine the actual wavelet shape. From an enlargement of Fig. 3, normals to a wave W_i were constructed. These normals were found to cross the jet centerline at nearly the same point P_i, and the radii r_i corresponding to W_i were equal. The wave front, therefore, was almost spherical in shape, and P_i was identified as its emission point (see Fig. 8 for details of construction). Thus, the predominant discrete radiation pattern consists of essentially spherical waves whose wavelength is equal to the axial distance between emission points as well as the distance between two adjacent wavelets, i.e., $\lambda_R = \langle P_iP_{i-1}\rangle = r_i - r_{i-1}$. Applying this method to successive wavelets, the wavelength was again found to be nearly equal to the jet diameter to within the deviation shown in Table 1.

b. Intensity of radiated wavelets

The decibel intensity l_R of a compression wave of excess pressure Δp is given by

$$l_R = 20 \log(\Delta p/\Delta p_l) + 10 \log(\rho_s a_s/\rho_2 a_2) \qquad (6)$$

where the threshold noise level $\Delta p_l = 0.0002$ dynes/cm^2 at standard density ρ_s and sound speed a_s. The second term in Eq. (6) accounts for the reduced decibel intensity of a compression wave behind the shock front since $\rho_s a_s/\rho_2 a_2 < 1$. However, for the range of shock strengths used this second term was of the order of 1% of the first and therefore neglected. Assuming the radiated wavelets to be very weak $\Delta p/p_2 = \gamma\, \Delta\rho/\rho_2$, and from Eq. (6) $l_R = 20 \log\gamma\, p_2\, \Delta\rho/\rho_2 \Delta p_l = 20 \log\gamma S p_1 \Delta\rho/\rho_2 \Delta p_l$. The quantity $\Delta\rho/\rho_2$ was evaluated from the interferograms by the integration procedure already described in the section entitled Experimental Procedures and Conditions. The intensity l_R vs the angular location θ (Fig. 8) of three consecutive waves (interferogram Fig. 3) is shown in Fig. 9.

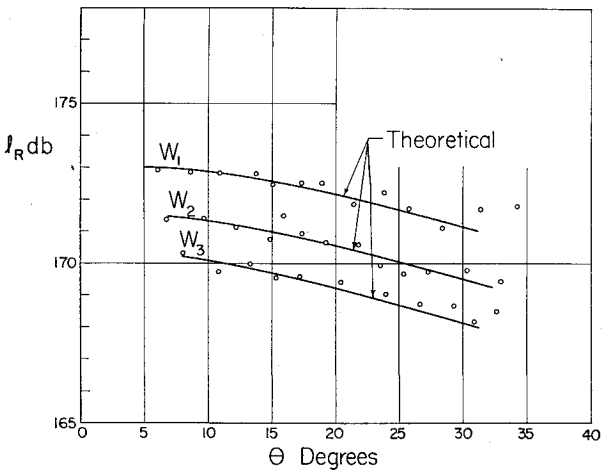

Fig. 9 Intensity and decay of successive compression waves (interferogram Fig. 3)

The attenuation of decibel intensity with increasing r_i and increasing θ is evident. Lighthill[17] has shown that the intensity [$I \propto (\Delta p)^2$] of sound emission from a moving point source P_i varies as $[r_i\,(1 - M_{2u}\cos\theta)]^{-2}$, where M_{2u} is the source convection velocity u_{2u} divided by the local speed of sound a_{2u}. Starting with the maximum measured value of l_R (173 db), the decay of intensity of each wave with r and θ was calculated. Good agreement with experimental results is evident (Fig. 9). Small differences may be attributed to local nonsphericity of the wavelets due to their initial passage through the nonuniform jet flow region, and loss of accuracy of fringe jump measurements with increasing θ due to the changing orientation of the fringes along the wavelets.

An attempt was made to ascertain the emission mechanism of the discrete wavelets. The jet flow turbulence can be excluded as the direct cause of the discrete radiation, as its overall intensity is concentrated within a frequency range much lower than the observed frequency of the discrete radiation (Table 1). It is suggested, therefore, that some mechanism involving characteristic flow oscillations of the interacted jet flow may be responsible for the intermittent wave system. An examination of the flow field immediately behind the shock bulge revealed the presence of an extended conical shock surface and a high-pressure region with lateral extent nearly equal to the jet diameter (Fig. 4). The longitudinal extent of this high-pressure region is also nearly equal to 1 jet diameter (Fig. 6b). The shock bulge is disturbed by the passage of the jet flow eddies, resulting in local pressure and velocity fluctuations. These in turn disturb the extended shock cone and adjacent high-pressure region. This may actuate an oscillation of the high-pressure region with a characteristic frequency corresponding to wavelength $\lambda_R \approx d$. Also the propagation of the compression waves over the shock bulge surface will disturb it and in turn may further perpetuate the oscillation of the high-pressure flow region. The emission mechanism of the superimposed pattern of numerous weak wavelets appears to be related directly to the passage of the small-scale jet flow eddies through the shock bulge.

References

[1] Lighthill, M. J., "On the energy scattered from the interaction of turbulence with sound or shock waves," Cambridge Phil. Soc. **49**, Part III, 531–551 (July 1953).

[2] Ribner, H. S., "Convection of a pattern of vorticity through a shock wave," NACA TN 2864 (1953).

[3] Ribner, H. S., "The sound generated by interaction of a single vortex with a shock wave," Univ. Toronto Inst. Aerophys. Rept. 61, AFOSR-TN 59-1166 (June 1959).

[4] Werner, J. F., "Unsteady interaction of a shock wave with a cellular vortex field," J. Fluid Mech. **10**, Part II, 195–208 (March 1961).

[5] Powell, A., "On the noise emanating from a two-dimensional jet above the critical pressure," Aeronaut. Quart. IV, Part II, 103–122 (February 1953).

[6] Powell, A., "On the mechanism of choked jet noise," Proc. Phys. Soc. 866, 1039 (1953).

[7] Lam, S. H., "Interaction of two-dimensional inviscid incompressible jet facing a hypersonic stream," Princeton Univ. AFOSR-TN-59-274 Rept. 447 (March 1959).

[8] Stalder, J. R. and Inouye, M., "A method of reducing heat transfer to blunt bodies by air injection," NACA RM A56B27a (May 17, 1956).

[9] Charzenko, N. and Hennessey, K., "Investigation of a retrorocket exhausting from the nose of a blunt body into a supersonic free stream," NASA TN-D-751 (September 1961).

[10] Romeo, D. J. and Sterett, J. R., "Exploratory investigation of the effect of a forward facing jet on the bow shock of a blunt body in a Mach number 6 free stream," NASA TN D-1605 (February 1963).

[11] Dosanjh, D. S., "Experiments on interaction between a traveling shock wave and a turbulent jet," J. Aeronaut. Sci. 24, 838–844 (1957).

[12] Dosanjh, D. S., "Use of a hot wire anemometer in shock tube investigations," NACA TN 3163 (December 1954).

[13] Dosanjh, D. S. and Weeks, T. M., "Interaction of traveling shock wave with turbulent flow fields," Syracuse Univ. Final Rept. ME552-6204F; also Armed Services Tech. Info. Agency AD 275 631 (April 1962).

[14] Weeks, T. M., "Interaction of traveling shock wave with opposing axisymmetric turbulent jet," Master's Thesis, Dept. Mech. Eng., Syracuse Univ. (January 1961).

[15] Rouse, H. (ed.), *Advanced Mechanics of Fluids* (John Wiley and Sons, 1959), Chap. VIII, Sec. D.

[16] Kuethe, A. M., "Investigations of the turbulent mixing regions formed by jets," J. Appl. Mech. 2, no. 3, A 87–95 (September 1935).

[17] Lighthill, M. J., "On sound generated aerodynamically II," Proc. Roy. Soc. (London) 222A, 1–32 (1954).

JULY 1963 AIAA JOURNAL VOL. 1, NO. 7

Constant Convective Heating Rate Surfaces for Lifting Re-Entry Vehicles

WILBUR L. HANKEY JR.* AND LAWRENCE E. HOOKS†
Aeronautical Systems Division, Wright-Patterson Air Force Base, Ohio

A constant emissivity surface of known area is considered. It is assumed that heat input to the surface is balanced by radiation to space. The minimum peak temperature possible on this surface occurs when the surface temperature is constant. It is shown that constant temperature is equivalent to constant local heating rate. Constant convective heating rate contours are determined by setting Lees' 1956 equation for laminar heating rate distribution equal to unity and solving for the surfaces that satisfy that condition. The resulting nose and leading edge geometries are presented for a ratio of specific heats of 1.2. Stagnation region heating rates and temperatures for constant convective heating rate surfaces and circular arc surfaces are compared at the same flight condition. Stagnation heating rates on the constant convective heating rate surfaces are approximately 70% of the values on circular arc surfaces fitting the same vehicle.

Nomenclature

A = area
K = a constant of proportionality
n = 0 for a planar body, 1 for a body of revolution
P = local static pressure
$\overline{Pr}$ = average Prandtl number
q = local heat transfer rate per unit area
Q = total heat transfer rate
R = local radius of curvature
S = distance along body surface from stagnation point
T = absolute temperature
V = local inviscid gas velocity, tangent to the body except when freestream conditions are indicated
x = distance along body axis from stagnation point
y = distance from body axis to body surface
β = dimensionless stagnation point velocity gradient, $(1/V_\infty)$, $(dV_\delta/d\theta)_S$ equal to $\{(\gamma - 1)/\gamma\}^{1/2}$
γ = effective ratio of specific heats
ϵ = emissivity
θ = angle between tangent plane at local body point and tangent plane at the stagnation point
μ = absolute viscosity
σ = Stephan-Boltzmann constant
ω = μ/RT

Subscripts

a = conditions at point where sonic velocity occurs
c = conditions on a surface with circular arc cross section
E = conditions on a surface with an elliptical cross section
0 = condition at the termination of constant heating rate surface
S = stagnation point conditions
δ = conditions at outer edge of boundary layer
∞ = freestream conditions

Received by ARS October 11, 1962; revision received May 9, 1963.

* Chief, Aerodynamics Branch, Dyna-Soar System Program Office.

† Physicist, Aerothermodynamics Unit, Flight Dynamics Laboratory.

I. Introduction

RE-ENTRY vehicles may be classed as ballistic vehicles or lifting vehicles. Ballistic vehicles are characterized by short re-entry time and turbulent boundary layer during the critical heat pulse. Lifting vehicles have a long re-entry time and laminar boundary layer during their critical heat pulses.

The flight corridor of either type of re-entry vehicle is limited by its ability to absorb or reject the re-entry heat load. The heat pulse applied to a ballistic vehicle during re-entry is of such short duration that cooling by ablation allows the vehicle to survive. Because of long re-entry times, however, it is probable that lifting re-entry vehicles will rely on cooling by reradiation over significant portions of their flight paths.